A neuromechanical model of multiple network oscillators for forward locomotion in *C. elegans*

Erick Olivares, Eduardo J. Izquierdo, Randall D. Beer

Cognitive Science Program, School of Informatics, Computing, and Engineering, Indiana University, Bloomington, USA

Abstract Multiple mechanisms contribute to the generation, propagation, and coordination of rhythmic patterns necessary for locomotion in *Caenorhabditis elegans*. Current experiments have focused on two possibilities: pacemaker neurons and stretch-receptor feedback. Here, we focus on whether locomotion behavior can be produced by a chain of network oscillators in the ventral nerve cord. We use a simulation model to demonstrate that a repeating neural circuit identified in the worm's connectome can be chained together to drive forward locomotion on agar in a neuromechanical model of the nematode, in the absence of pacemaker neurons or stretch-receptor feedback. Systematic exploration of the space of possible solutions reveals that there are multiple configurations that result in locomotion that match the kinematics of the worm on agar. Analysis of the best solutions reveals that gap junctions between different classes of motoneurons are likely to play key roles in coordinating oscillations along the ventral nerve cord.

Introduction

Understanding how behavior is generated through the interaction between an organism's brain, its body, and its environment is one of the biggest challenges in neuroscience (***Chiel and Beer, 1997***; ***Chiel et al., 2009***; ***Krakauer et al., 2017***). Understanding locomotion is particularly critical because it is one of the main ways that organisms use to interact with their environments. Moreover, locomotion represents a quintessential example of how behavior requires the coordination of neural, mechanical, and environmental forces. *Caenorhabditis elegans* is an ideal candidate organism to study the neuromechanical basis of locomotion because of the small number of neurons in its nervous system and the reconstruction of its neural and muscle anatomy at the cellular level (***White et al., 1986***; ***Varshney et al., 2011***; ***Cook et al., 2019***). However, despite the available anatomical knowledge, how the rhythmic patterns are generated and propagated along the body during forward locomotion on agar is not yet fully understood (***Cohen and Sanders, 2014***; ***Gjorgjieva et al., 2014***; ***Zhen and Samuel, 2015***).

As with many other organisms, there are likely multiple mechanisms, internal and external, contributing to the generation, propagation, and coordination of rhythmic patterns controlling locomotion in *C. elegans* – a robust blend of central pattern generators and sensory reflexes (***Rossignol et al., 2006***). Until recently, the majority of experimental work on *C. elegans* locomotion had been focused on understanding the role of external contributions, specifically the role of stretch-receptor feedback. The proposal that stretch-receptor feedback plays an important role in the generation of movement in the nematode dates back to the time of the original reconstruction of the connectome (***White et al., 1986***). There has since been evidence of mechanically gated channels

that modulate *C. elegans* locomotion (***Tavernarakis et al., 1997***), as well as evidence of a direct relationship between body curvature and neural activity (***Wen et al., 2012***). However, coordinated rhythmic patterns can also be produced internally, while remaining open to modulation through external contributions. Central pattern generators (CPGs) are known to be involved in a wide variety of behaviors in a number of different organisms, including insect flight, swimming in molluscs, gut movements in crustaceans, and swimming and respiration in vertebrates (***Marder and Bucher, 2001***; ***Goulding, 2009***; ***Katz, 2016***; ***Arshavsky et al., 2016***; ***Dasen, 2018***; ***Minassian et al., 2017***). In a CPG, the rhythmic pattern can be generated through the intrinsic oscillatory properties of pacemaker neurons or it can emerge from the interaction of networks of non-oscillatory neurons (***Goulding, 2009***). Recent experiments have provided support for the role of intrinsic oscillations in *C. elegans* locomotion (***Gao et al., 2018***; ***Fouad et al., 2018***; ***Xu et al., 2018***). Although the work attributes the source of these rhythm generators to pacemaker neurons, the evidence provided does not discard the possibility of network oscillators (***Wen et al., 2018***).

It is increasingly acknowledged that simulation models play an important role in elucidating how brain-body-environment systems produce behavior (***Ijspeert, 2008***; ***Abbott, 2008***; ***Izquierdo, 2018***). In *C. elegans*, there has been an surge of theoretical work focused on understanding the neuromechanical basis of locomotion. Several computational models have demonstrated that proprioception alone can be used to generate rhythmic patterns and propagate them along the body (***Niebur and Erdös, 1991***; ***Karbowski et al., 2008***; ***Boyle, 2009***; ***Mailler et al., 2010***; ***Wen et al., 2012***; ***Izquierdo and Beer, 2018***; ***Fieseler et al., 2018***; ***Gleeson et al., 2018***). There have also been a number of models that have considered the potential role of CPGs in *C. elegans* locomotion (***Deng and Xu, 2014***; ***Palyanov et al., 2018***; ***Denham et al., 2018***; ***Kunert et al., 2014***). Some of these models have considered a CPG in the head circuit (***Izquierdo and Beer, 2018***) or in the command interneurons (***Deng and Xu, 2014***). Some of the models show how sinusoidal functions alongside the ventral nerve cord can drive a mechanical body to produce movement (***Palyanov et al., 2018***; ***Denham et al., 2018***). Only a few studies have considered the generation of rhythmic patterns from network oscillators in neuroanatomically-grounded models of the ventral nerve cord (***Kunert et al., 2014***; ***Olivares et al., 2018***). However, these models have not considered the dynamic interaction of these neural patterns with the mechanical body and environment to produce movement.

Current models have left a major question unanswered: Can multiple network oscillators in the ventral nerve cord coordinate their activity to produce the traveling wave necessary for forward locomotion in the absence of either pacemaker neuron activity or stretch-receptor feedback? In this paper, we present a model of multiple network oscillators driving forward locomotion grounded in the neurobiology, anatomy, and biomechanics of the worm. The model integrates multiple repeating neural units in the VNC based on a statistical analysis of the available connectome data (***Haspel and O'Donovan, 2011***). Motoneurons innervate an anatomically grounded model of the muscles. The neuromuscular system is embedded in a model of the biomechanics of the worm's body (***Boyle et al., 2012***). We used an evolutionary algorithm to explore the space of unknown parameters of the VNC motoneuron such that the integrated neuromechanical model matched the speed of the worm during forward locomotion on agar. The models closely resemble the kinematics of movement and the effect on behavior of manipulations in the neurons and body observed for forward locomotion studies in the worm (***Fouad et al., 2018***; ***Xu et al., 2018***). The models demonstrate that coordination across neural units in the VNC can be achieved by the electrical synapses and that the coordination can happen in the anterior and posterior direction. Detailed analysis of the operation of the model sheds further light on the mechanisms that can generate and propagate oscillations in the worm and leads to a number of experimental predictions.

Results

Multiple CPGs can coordinate to produce forward locomotion in the worm

In previous work, we demonstrated the theoretical feasibility of a CPG in a small repeating subcircuit of the ventral nerve cord without pacemaker neurons (***Olivares et al., 2018***). Can this repeating circuit coordinate oscillations across the complete length of the worm to produce not just a dorsoventral oscillation, but a propagating wave in the absence of stretch-receptor feedback? In order to address this question, we modeled an extended version of the circuit that includes all VNC motoneurons, intra-unit (black) and interunit (red) chemical and electrical connections (Fig. 1). We embodied and situated the model circuit within the model muscles, model body, and model agar environment, while deliberately leaving out stretch-receptor feedback. Then, we used a stochastic optimization technique to search for configurations of the circuit's parameters that reproduced forward locomotion. Despite the absence of stretch-receptor feedback, when simulated, all selected model worms exhibited regular dorsoventral bends that propagated from head to tail (see example of one model worm in Fig. 2). In other words, the search consistently found configurations of the neuroanatomical circuit that could produce forward locomotion through the coordination of multiple central pattern generators along the ventral nerve cord. This provides a theoretical demonstration of the feasibility of the multiple CPG hypothesis.

Behavior of model worms matches the behavior of the worm

The behavior of the model worms matches the behavior of the worm in a number of important ways. First, the instantaneous velocity of model worms oscillates around 0.2mm/s (see example from one model worm in Fig. 2B). This was the value used to fit the model during the evolutionary search based on the broad range observed experimentally (***Cronin et al., 2005***; ***Omura et al.,***

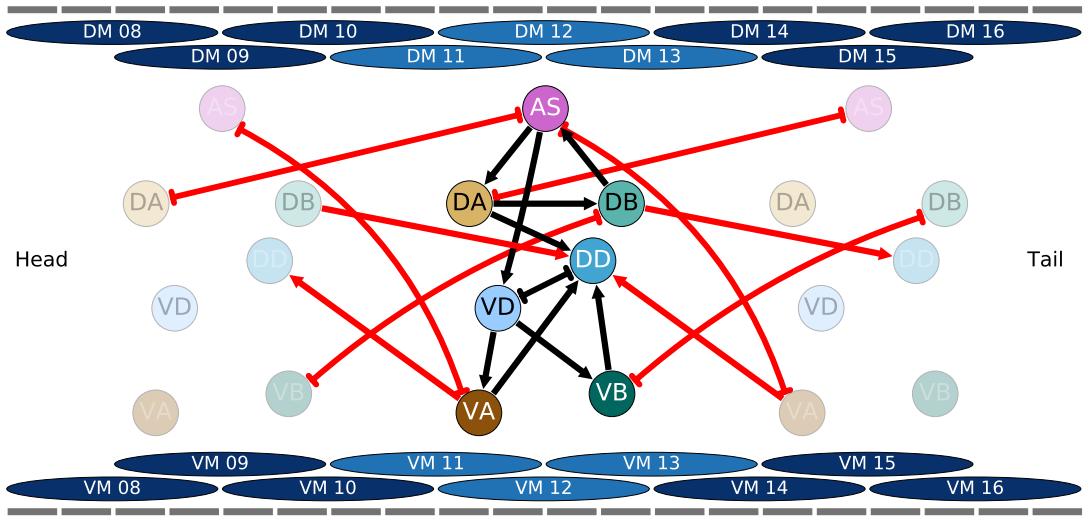

Figure 1. Neuromechanical model. The model of the body is a reimplementation of the model presented by ***Boyle et al.*** (***2012***). Dorsal and ventral lateral elements from the biomechanical model of the body are represented in gray on the top and bottom of the figure, respectively. Following previous work (***Izquierdo and Beer, 2018***), are modeled as elements that lie along the cuticle that can contract and relax in the dorsoventral plane and that are staggered along the ventral and dorsal sides of the worm (blue ovals). Muscle force is distributed across all lateral elements they intersect. We modeled the motoneurons in the ventral nerve cord as a network composed of seven identical subunits. We relied on a statistical analysis of the motoneurons in relation to the position of the muscles they innervate to identify the most common connections (***Haspel and O'Donovan, 2011***). One of seven repeating neural subunits is shown in complete detail. Intraunit connections are shown in black. Interunit connections are shown in red. Chemical synapses are shown with arrows. Gap junctions are shown as connections with line endings. All subunits innervate three ventral and dorsal muscles, except the most anterior and the most anterior subunits which innervate four muscles.

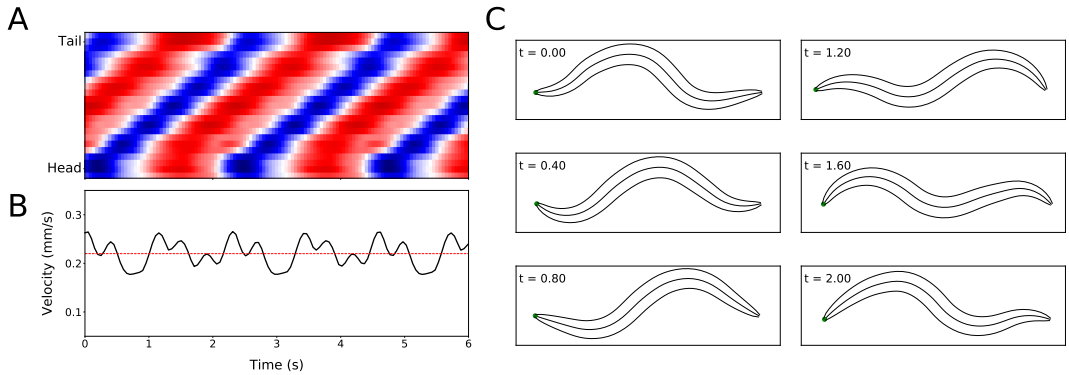

Figure 2. Locomotive behavior of model worms resembles forward locomotion of worms on agar. Example from one model worm from the ensemble of solutions. [A] Kinogram from one filtered individual showing dorsoventral bending along time (x-axis) and body (y-axis). The intensity of red and blue depict dorsal and ventral bending, respectively. [B] Instantaneous velocity of the body center of mass (black trace) in relation to average velocity used for the fitness function (red line). [C] Worm body posture at different points in time (in seconds) shows propagating wave.

2012; ***Machino et al., 2014***). Second, the solutions were filtered to only those that matched the kinematic properties observed during crawling by the wild-type worm, including a wavelength between 0.7 and 0.9 of the worm's body length (***Shen et al., 2012***; ***Pierce-Shimomura et al., 2008***; ***Fang-Yen et al., 2010***). Finally, solutions were also filtered to match the relative importance of the B-class motoneurons over the A-class motoneurons observed experimentally during forward locomotion (***Chalfie et al., 1985***; ***Faumont et al., 2011***; ***Kawano et al., 2011***; ***Haspel et al., 2010***). Altogether, we found 15 different model configurations that reproduced forward locomotion on agar using multiple coordinating CPGs along the body and that satisfy all of the selection criteria.

A number of recent experiments (***Fouad et al., 2018***; ***Xu et al., 2018***) have provided support for the theoretical demonstration that neuroanatomically-grounded CPGs in the ventral nerve cord could be involved in aspects of forward locomotion in the worm (***Olivares et al., 2018***). In this section, we examine the different ways in which the model worms are consistent with what has been observed in those experiments.

Rhythmic posterior undulations persist despite anterior paralysis

Recent experiments have provided evidence that posterior dorsoventral bending persists despite anterior paralysis and suppression of stretch receptor activity (***Fouad et al., 2018***; ***Xu et al., 2018***). The model presented here is consistent with this experimental finding. In order to demonstrate this, we replicated the experimental condition on the model worms in two ways. First, we suppressed the neuromuscular junction activity for the three anterior-most neural units. Second, we silenced the neural activity of all neurons in those same three anterior-most neural units. Note that taking into consideration the suppression of stretch-receptor feedback was not necessary given that this model did not include stretch-receptor feedback. We examined the resulting kinematics of movement under both conditions. Specifically, we measured the magnitude of the amplitude of dorsoventral oscillations in the head and the tail. In both conditions, we observed a sharp reduction in dorsoventral bending in the head, but only a slight reduction of dorsoventral bending in the posterior regions of the body in all 15 solutions (Fig. 3A). Furthermore, coordination of the multiple oscillators in the posterior part of the body remained intact (see example from one model worm in Fig. 3B). Therefore, as with the worm, posterior dorsoventral bending persists in model worms despite anterior paralysis.

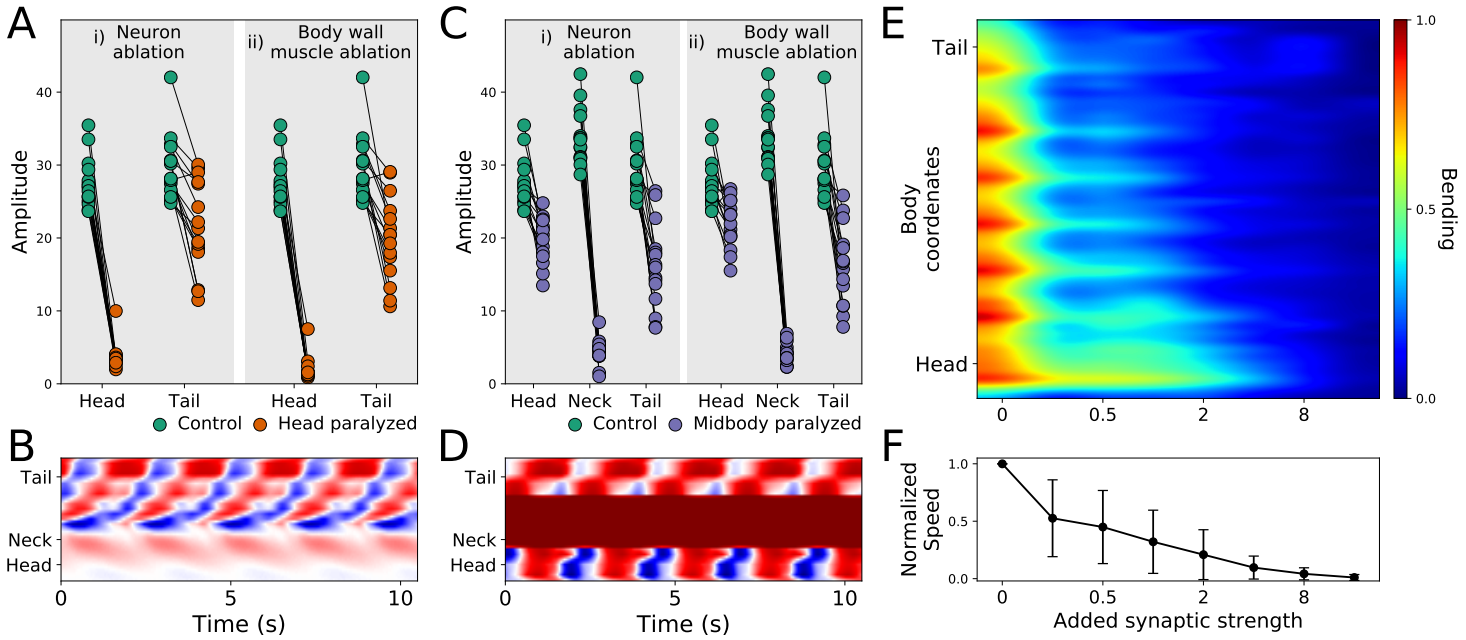

Figure 3. Filtered models are consistent with recent experimental observations. [A] Rhythmic posterior undulation persists despite anterior paralysis. Total bending amplitude (y-axis) evaluated as in previous work (***Fouad et al., 2018***). [i] When motoneurons in the head are ablated, bending amplitude in the head decreases but not in the tail. [ii] Similarly, when body-wall muscles (BWM) in the head are inactivated, bending amplitude in the head decreases but not in the tail. Therefore, paralysis in the head does not abolish bending in the tail. [B] Example kinogram from one model worm shows bending over time when neuromuscular junctions in the head are inactivated. [C] Rhythmic undulation persists simultaneously in the head and the tail despite midbody paralysis. [i] When motoneurons in midbody are ablated, bending amplitude decreases in the midbody but not in the head or the tail. [ii] Similarly, when body-wall muscles (BWM) in the midbody are inactivated, bending amplitude decreases in the midbody but not in the head or the tail. Therefore, midbody paralysis demonstrates that head and tail are capable of simultaneous and uncoordinated oscillations. [D] Example kinogram from one model worm shows bending over time when neuromuscular junctions in the midbody are inactivated. [E] Overexpression of electrical synapses on B-class motorneurons induce complete body paralysis. Overexpression was simulated by increasing the synaptic strength of B-class gap junctions: VB⊣DB^{+1}, DB⊣DB^{+1}, VB⊣VB^{+1}. [F] Speed as a function of gap junction overexpression in the model worms. The disks represent the mean and the bars represent the standard deviation. As the synaptic strength of the B-class gap junctions is increased, the speed of the model worms decreases.

Head and tail are capable of simultaneous and uncoupled oscillations

Recent experiments have also provided evidence that the head and the tail are capable of simultaneously producing uncoupled oscillations (***Fouad et al., 2018***). Our model is consistent with this experimental finding. To demonstrate this, we again replicated the experimental condition in two ways. First, we suppressed the neuromuscular junction activity for the three mid-body neural units. Second, we silenced the neural activity of all neurons in those same three mid-body neural units. In both conditions, we observed that suppressing mid-body components did not eliminate body bending in either the head or the tail (Fig. 3C). In other words, like in the worm, uncoupled dorsoventral oscillations were present simultaneously in the head and the tail (see example from one model worm in Fig. 3D). Unlike the experimental observations (***Xu et al., 2018***; ***Fouad et al., 2018***), the oscillations in the head and the tail have the same frequency. This is expected because this model does not consider a separate head circuit (we consider the head circuit in a separate model (***Izquierdo and Beer, 2018***).

Strengthening gap junctions in B-class motorneurons impairs locomotion

Finally, recent experiments have provided evidence that strengthening the gap junctions (via genetic overexpression of UNC-9, one of the genes responsible for gap junctions in *C. elegans*) in the B-class motor neurons leads to constitutive paralysis in the worm (***Xu et al., 2018***). Our model is also consistent with this finding. To demonstrate this, we systematically increased the synaptic weight of the gap junctions interconnecting B-class motorneurons (both the $VB \dashv DB^{+1}$, $VB \dashv VB^{+1}$ and $DB \dashv DB^{+1}$) and measured the resulting bending along the body and speed of the model worm. As the strength of the gap junctions was increased, the bending in the body decreased. Noticeably, the effect was more pronounced in the tail than in the head (Fig. 3E). Accordingly, the velocity of the simulated worms also decreased as the strength of the gap junctions was increased, leading ultimately to total paralysis (Fig. 3F). Therefore, as with the worm, overexpression of the B-class gap junctions leads to paralysis.

Mechanisms of oscillation and coordination in the ensemble of model worms

In the previous section we provided evidence that the simulated model worms can produce locomotion without stretch receptors and without pacemaker neurons in a way that both resembles the kinematic characterization of the worm's forward movement on agar and is consistent with key findings from various experimental manipulations. This suggests that the way these model worms operate could be illustrative for understanding the mechanisms responsible for locomotion in the worm. Two basic mechanisms are necessary for a chain of CPGs to drive locomotion in the worm. First, a network of neurons must be able to generate oscillations intrinsically. Second, adjacent CPGs must coordinate oscillations with the appropriate phase delay along the anteroposterior axis. In what follows, we examine the model worms in detail to answer the following two key questions: How do the model worms generate dorsoventral oscillations? And how do they coordinate these oscillations across the length of the body to generate a propagating wave capable of producing thrust against an agar surface? Answering these questions in the model worms will offer hypotheses for how the worm might accomplish the same feats.

Model worms use the dorsal AS-DA-DB subcircuit to generate oscillations

How do these model worms generate oscillations? To answer this question, we first determined which set of neurons are involved in producing oscillations. For a subcircuit to be capable of generating oscillations in the absence of pacemaker neurons, a recurrently connected set of neurons are required. There are three possible subcircuits in the VNC unit that are capable of generating intrinsic network oscillations: AS-DA-DB, VD-VA-DD, and VD-VB-DD (Fig. 4A). We examined whether each of these subcircuits alone could produce oscillations (Fig. 4B). We measured the total change in neural activity as an indicator of oscillations. Because the subcircuits were evaluated in isolation from the rest of the network, we examined each of them with a wide range of compensatory tonic

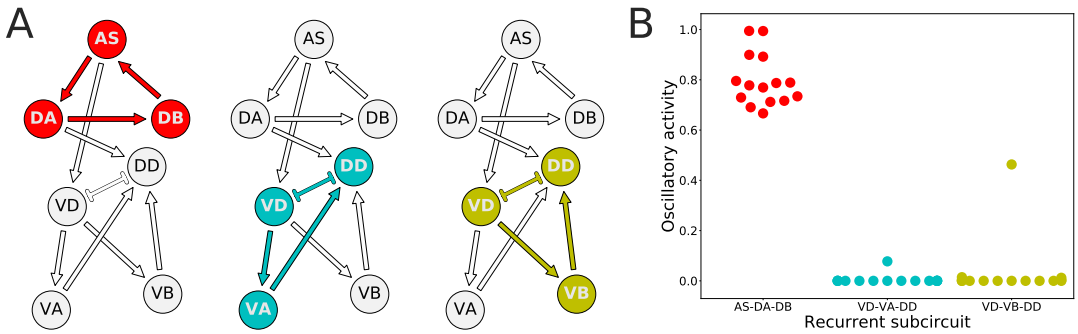

Figure 4. Oscillations originate primarily in the dorsal core subcircuit: AS-DA-DB. [A] Subcircuits within each neural unit where network oscillations are possible. [B] Ability to oscillate when each of these circuits is isolated.

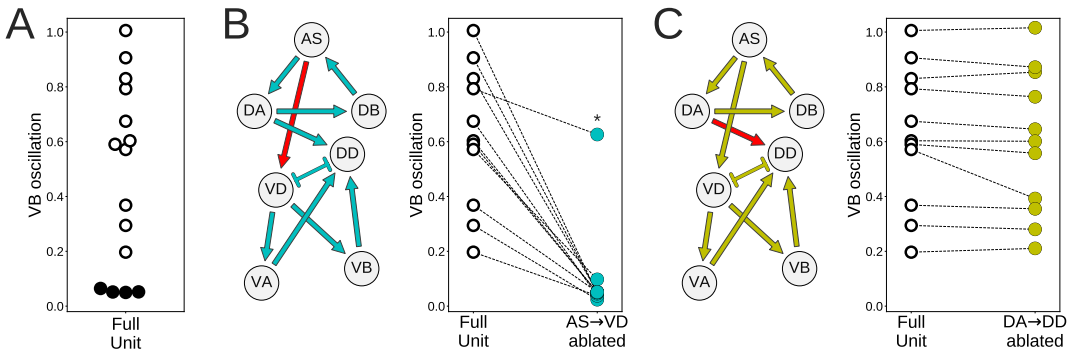

Figure 5. Model worms use the AS→VD connection to propagate the oscillation to the ventral motoneurons. [A] Oscillation in VB motoneurons. Four solutions do not exhibit oscillations in VB (solid black). [B] Oscillation in VB is abolished when the connection AS→VD is ablated (connection shown in red). This is true in all solutions, except M11 (shown with an asterisk), which shows intrinsic oscillations in the ventral subcircuit. [C] Oscillation in VB persists when the connection DA→DD is ablated (connection shown in red).

input to each neuron. Consistent with our previous work in the isolated neural unit (***Olivares et al., 2018***), all model worms generated oscillations in the AS-DA-DB subcircuit. Out of the 15 model worms examined, only one of them (solution M11) generates oscillations also in the VD-VB-DD subcircuit and only one (solution M6) generates weak oscillations in the VD-VA-DD subcircuit.

Model worms use the AS→VD connection to propagate the oscillation to the ventral motoneurons

Despite the primary role of the dorsal motoneurons in the generation of oscillations, all model worms show ventral neural oscillatory activity. In the majority of model worms (11 out of 15), the ventral motoneurons in an isolated subunit can oscillate (Fig. 5A). How does the oscillation propagate to the ventral motoneurons in these model worms? There are two possibilities: the AS→VD or the DA→DD chemical synapses. We examined whether the ventral B-class motoneuron could produce oscillations when either of those connections was ablated (Fig. 5). In 10 out of the 11 solutions the AS→VD (and not the DA→DD) synapse was necessary to propagate the oscillations from the dorsal core (Fig. 5B,C). This is consistent with our previous work in the isolated neural unit (***Olivares et al., 2018***). In one of the model worms (solution M11), neither of the connections were necessary. Recall from the previous section that this solution was the only one that also generated strong oscillations in the ventral side. There are four solutions where the ventral motoneurons do not oscillate in the isolated subunit. In these solutions, ventral motorneurons oscillate due to interunit contributions.

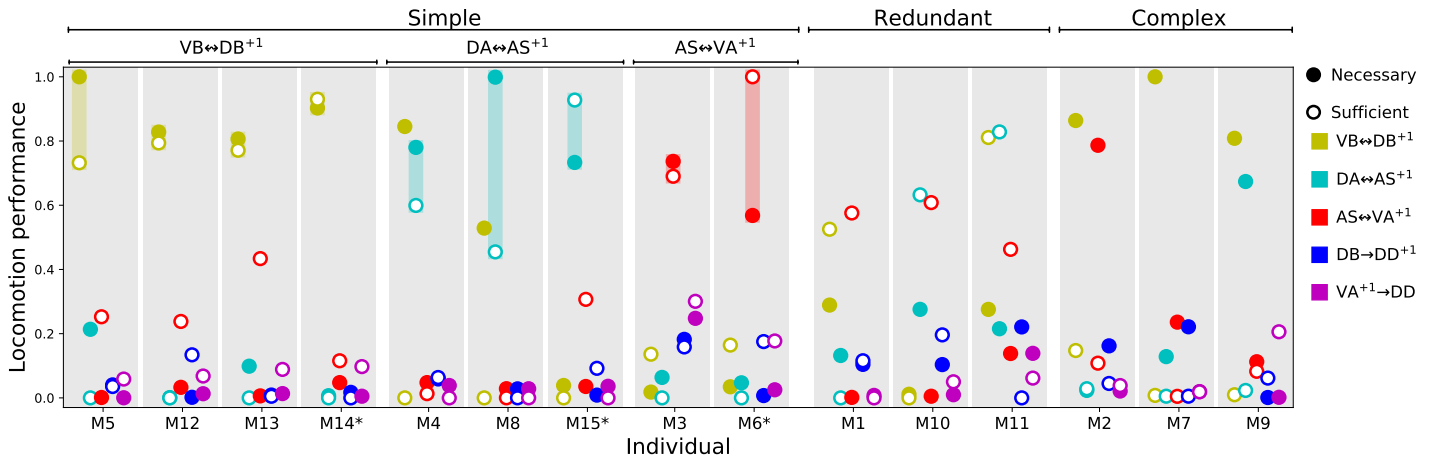

Figure 6. Necessity and sufficiency of each interunit connection to coordinate oscillations for locomotion in each of the model solutions. Each of the 15 solutions (labeled M1-M15) are shown on the x-axis. On the y-axis is the locomotion performance of each solution as a result of examining each of their interunit connections (labeled by color, see legend) for necessity and sufficiency. To evaluate necessity, we ablated the connection in question and examined the worm's ability to move forward (solid disks). To evaluate sufficiency, we ablated all but the connection in question and again examined the worm's ability to move forward (circles). Analysis of all 15 solutions revealed three categories of strategies for coordination. "Simple" solutions correspond to those in which a single gap junction is both necessary and sufficient to coordinate the chain of oscillators that drive locomotion. These group of solutions are further subdivided based on which of the three gap junctions is responsible for coordinating the subunits: VD⊣DB^{+1}, DA⊣AS^{+1}, and AS⊣VA^{+1}. "Redundant" solutions are those in which more than one solution is sufficient to drive locomotion. "Complex" solutions are those in which no single gap junction is responsible for coordinating between units. Asterisks in the x-axis label mark the solutions with the highest single sufficient connection from each of the solutions in the "Simple" groups.

Oscillations coordinate through a combination of three key interunit gap junctions: AS-VA^{+1}, DA-AS^{+1}, and VB-DB^{+1}

That the model worms move forward is evidence that the multiple CPGs along the body coordinate their activity. But how is the coordination between the different units achieved? To answer this question, we examined the necessity and sufficiency of each interunit connection, chemical and electrical (Fig. 6). In all the model worms examined, only the gap junctions played a role in coordinating oscillations among the different units in the VNC. The interunit chemical synapses were neither necessary nor sufficient for the coordination. In 9 of the 15 solutions examined, a single gap junction was both necessary and sufficient to coordinate the chain of oscillators to drive locomotion forward in the worm. The VD⊣DB^{+1} gap junction was necessary and sufficient to coordinate oscillations in four of the solutions; the DA⊣AS^{+1} gap junction was necessary and sufficient in three solutions; the AS⊣VA^{+1} gap junction was necessary and sufficient in two. These solutions are particularly interesting because of how *simple* they are (Fig. 6). We analyze one from each of these groups in more detail in the next section. There are three solutions where multiple single gap junctions are sufficient, but no single gap junction was necessary. These solutions use *redundant* mechanisms to coordinate (Fig. 6). Finally, there are three solutions where no single connection is sufficient but several of them are necessary. These solutions are the most *complex* of the ensemble because they rely on multiple gap junctions to coordinate (Fig. 6).

Analysis of individual representative solutions

To better understand how locomotion is generated in these evolved networks, we selected single individuals from the "simple" group to analyze in more detail. Individuals were selected based on the highest performance on the sufficiency test (i.e., solution M14 for VD⊣DB^{+1}, solution M15 for DA⊣AS^{+1}, and solution M6 for AS⊣VA^{+1}). Based on the results from the previous section, we simplified solutions to their minimal circuit configurations. Simulated models could still perform locomotion efficiently in these simplified configurations (Fig. 7A). In all three simplified solutions, the kinematics of movement exhibit an oscillation in the head that travels posteriorly in a way that

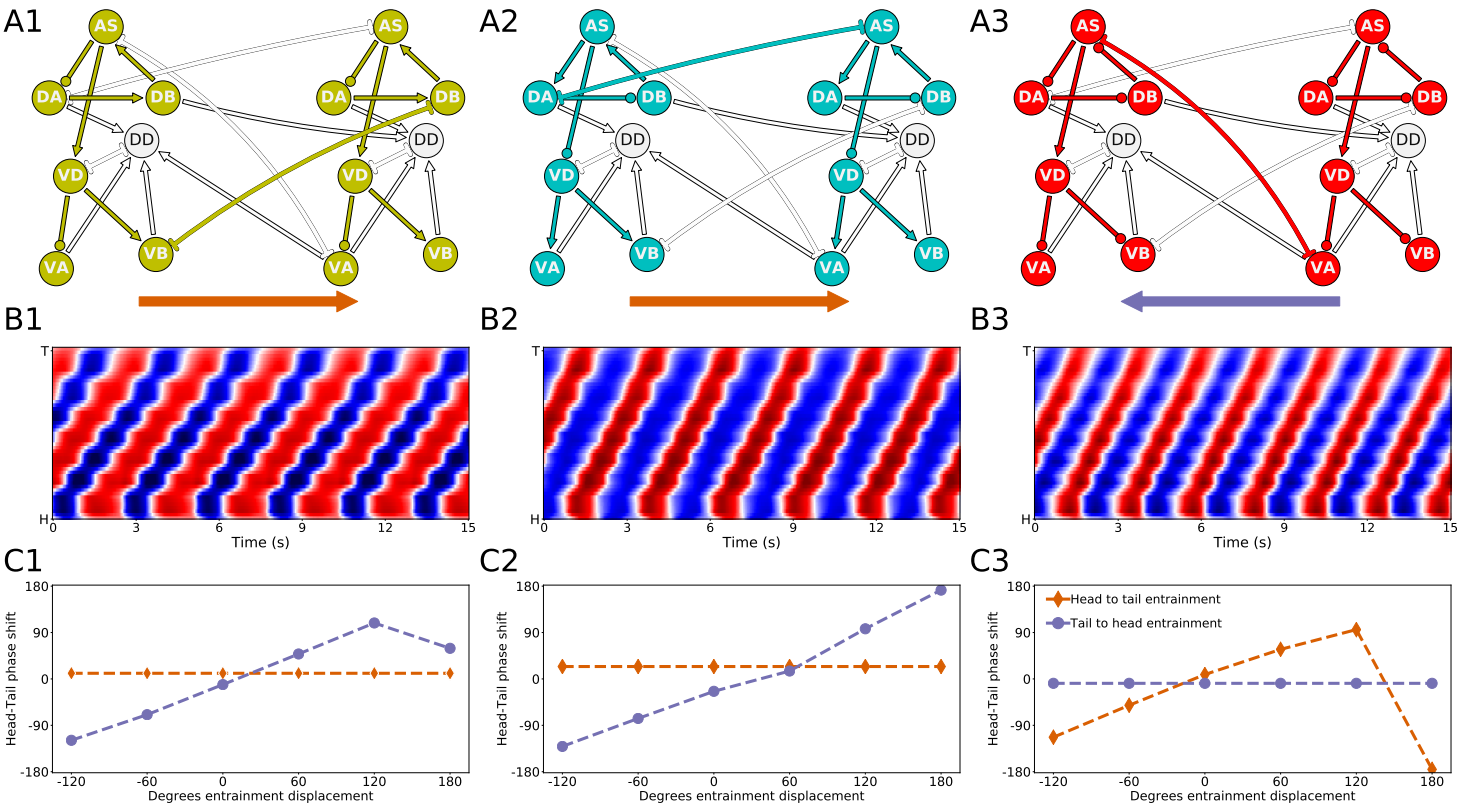

Figure 7. Mechanisms of anterior-posterior coordination. [A] Minimal network capable of driving locomotion in each of the solutions from the "simple" group: M14 for VD⊣DB^{+1} [A1], M15 for DA⊣AS^{+1} [A2], and M6 for AS⊣VA^{+1}) [A3]. Arrows represent excitatory chemical synapses. Connections ending in circles represent inhibitory chemical synapses. Connections with line endings represent gap junctions. [B] Kinograms for each of the minimal configurations above show coordinated bending waves through the body. [C] Entrainment analysis for each of the solutions reveals the directionality of the coordination among the subunit oscillators. The purple trajectory depicts the shift in phase that occurs in the posterior-most unit when the phase of the anterior-most unit is displaced. The brown trajectory depicts the shift in phase that occurs in the anterior-most unit when the phase of the posterior-most unit is displaced. In solutions M14 and M15, the anterior-most neural unit is capable of entrainning the posterior-most neural unit but not the other way around [C1, C2]. This suggests the coordination afforded by these two gap junctions is directed posteriorly. On the contrary, in solution M6, it is the posterior-most neural unit that is capable of entraining the anterior-most unit and not the other way around [C3]. This suggests the coordination afforded by this gap junction is directed anteriorly.

remains consistent with what has been observed in the worm (Fig. 7B). Because all three solutions can generate movement forward, we know that the multiple CPGs along the body coordinate to achieve the required phase shift. From the previous section we also know that an individual synapse is sufficient to coordinate the oscillations. In this section, we examine how the coordinated phase-shift is achieved in each of these solutions.

Directionality of coordination

The first thing we need to understand about coordination in these circuits is their directionality. Do anterior units influence the ones posterior to them, or vice-versa? Because the neural units along the VNC are coordinating their phases through gap junctions that allow for bi-directional communication, the directionality of coordination is not directly obvious.

First, in the solution that relies on the VB⊣DB^{+1} gap junction (Fig. 7A1), the anatomy suggests that the oscillation propagates posteriorly. This is because the interunit connection VD⊣DB^{+1} places the posterior CPG effectively downstream of the anterior CPG. The oscillation in the anterior dorsal core propagates ventrally. Then the VB⊣DB^{+1} gap junction coordinates the oscillation with the dorsal core unit immediately posterior to it. Therefore, in this solution, despite the bi-directionality of the coordinating gap junction, the anterior units are likely to be setting the phase of the posterior

ones, and not the other way around. In order to test this hypothesis, we performed an entrainment analysis. We introduced a shift in phase first in the anterior-most neural unit and then in the posterior-most neural unit, and we measured the degree to which the rest of the neural units adopted the new phase (Fig. 7C1). As expected, when the phase was shifted in the anterior-most unit, the rest of the body adopted that shift successfully; when the phase was shifted in the posterior-most unit, the rest of the body was unaffected.

Second, in the solution that relies on the ASI⊣VA^{+1} gap junction (Fig. 7A3), the anatomy suggests that the oscillation propagates anteriorly. This change in directionality is a result of the interunit connection ASI⊣VA^{+1} placing the anterior CPG downstream of the posterior one. The oscillation in the posterior dorsal core, once propagated ventrally, affects through the ASI⊣VA^{+1} gap junction the oscillation of the dorsal core in the unit immediately anterior to it. Therefore, opposite to the previous model worm, in this model worm the posterior units are likely to be setting the phase of the anterior ones, and not the other way around. This is again despite the bi-directionality of the coordinating gap junction. We tested this hypothesis using the same entrainment analysis as before (Fig. 7C3). As expected, when the phase was shifted in the anterior-most unit, the rest of the body was unaffected; when the phase was shifted in the posterior-most unit, the rest of the body adopted that shift successfully.

Finally, in the solution that relies on the DAI⊣AS^{+1} gap junction (Fig. 7A2), anatomy alone cannot tell us whether the coordination is occurring anteriorly or posteriorly. Because the connection is directly between the two CPGs (neither one is downstream of the other), and because the coordinating component is a bi-directional gap junction, the coordination can occur in either direction. We used the same entrainment analysis as before to examine the directionality of coordination in this model worm (Fig. 7C2). When the phase was shifted in the anterior-most unit, the rest of the body adopted that shift successfully; when the phase was shifted in the posterior-most unit, the rest of the body was unaffected. Thus, in this model worm the coordination of the shift occurs from head to tail.

Interunit phase-shift

The second aspect of the coordination that is crucial to understanding how locomotion is generated is the shift in phase between adjacent neural units. In order to examine this, we identified the approximate shift in phase that occurs at every step of the way from the DB neuron in one unit to the DB neuron in the adjacent unit (Fig. 8). We selected to measure the shift in phase between adjacent B-class neurons because of their primary role in forward locomotion. Although the neural dynamics in the model correspond to periodic oscillations, the specific shape of each neural activity is different. Because of the differences, we cannot relate the dynamic of two neurons as merely a shift in phase (i.e., $f(t) = g(t+T)$, where f and g are the dynamics of the two neurons). Nevertheless, we can approximate the shift in phase by assuming that the neurons in the model share the same oscillation frequency. This is the case particularly in the midbody subunits. For this analysis, we used units 3 and 4 to calculate the shift in phase. In order to estimate the phase of each neuron, we calculate the middle point between the maximum and minimum rate of change for one oscillation cycle for each neuron.

The highlighted neurons and connections for each network illustrates the shortest path from one DB to the DB in the adjacent neural unit in the direction of the transmission of information determined from the directionality analysis in the previous section. The first thing to note is that the path is different for each network (Fig. 8). Second, the shift in phase between two neurons is different among the different networks. For example, in one of the solutions (Fig. 8A), DB→AS is linked to an eight-degree shift in phase between DB and AS, whereas the same connection is linked to a 72-degree shift in phase in another network (Fig. 8B). However, despite the differences in how the model circuits operate at the level of pairwise neuron interactions, the shifts in phase from one complete neural unit to the one immediately posterior are relatively similar. It is key to note that it is this shift in phase from one unit to the next which is the primary functional activity of the network,

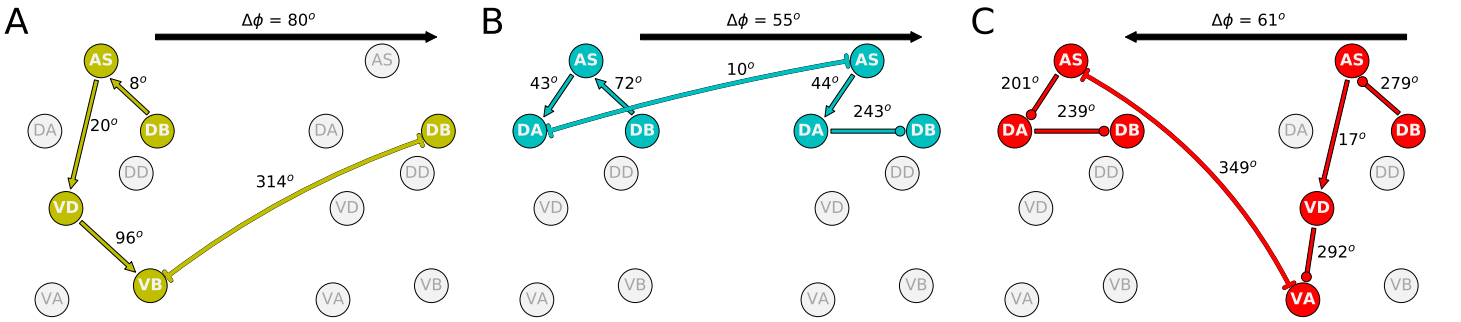

Figure 8. Phase delay among adjacent subunits in different networks. The highlighted neurons and connections for each network illustrates the shortest path from one DB to the DB in the adjacent neural unit in the direction of the transmission of information determined from the directionality analysis in the previous section. Despite large differences in how these different model circuits operate, the shift in phase from one unit to the one immediately posterior to it are relatively similar.

which ultimately leads to efficient forward locomotion on agar. This analysis suggests that high level of variability at the neuron-level implementation of solutions can result in similar functional results. To highlight this result, we examined the rest of the circuits in the "simple" networks. The phase shift measured between neurons DB→AS had a mean of 154.0 degrees and a standard deviation of 109.9. Yet, adjacent units had a mean phase shift of 54.4 with a standard deviation of only 8.9.

Interunit gap junctions present in connectome

It is important to recall that the repeating neural unit upon which we based our model is only a statistical summary of the VNC (***Haspel and O'Donovan, 2011***). In this section, we address how the key components that we have identified map onto the actual neuroanatomy of the worm. We examined the most recent reconstructions of the hermaphrodite and the male (***Varshney et al., 2011***; ***Jarrell et al., 2012***; ***Xu et al., 2013***; ***Cook et al., 2019***) for the existence of the three key interunit gap junctions responsible for coordinating the multiple oscillators in the model worms. We found that all three key components occur in a large portion of the ventral nerve cord in both hermaphrodites and males (Fig 9). Moreover, because the connectome reconstruction is still incomplete in the mid-body and posterior section of the VNC, additional connections are likely to be present in these regions. Although no single connection is present for every pair of adjacent units, there are combinations of different connections scattered throughout the full length of the ventral nerve cord. As observed in many of the evolved solutions, these three interunit gap junctions can work together to help coordinate oscillations. One thing to keep in mind is that not all of these connections are directed in the way we have idealized in the model. For example, although most AS⊣VA connections are directed posteriorly (i.e., with AS anterior to VA), in one of the connections the directionality is inverted (see posterior of the hermaphrodite). Assuming the directionality shown in the model, VB⊣DB and DA⊣AS will coordinate units posteriorly, and AS⊣VA will coordinate units anteriorly. Variability in the directionality in the connectome will have the effect of inverting the directionality of the coordination for those connections. Altogether, from these results, it seems plausible that multiple network oscillators in the ventral nerve cord could robustly coordinate their phases, even in the absence of stretch-receptor information, both anteriorly and posteriorly in the worm.

Discussion

We provide an existence proof that the multiple intrinsic network oscillators hypothesis for forward locomotion is feasible in a neuromechanical model of the worm. Our modeling strategy allowed us to find 15 model configurations that closely resemble the kinematics of movement and roles of key motoneurons observed during forward locomotion in the worm. Crucially, the models are consistent with recent experimental results that suggest the existence of multiple oscillations (***Fouad et al.,***

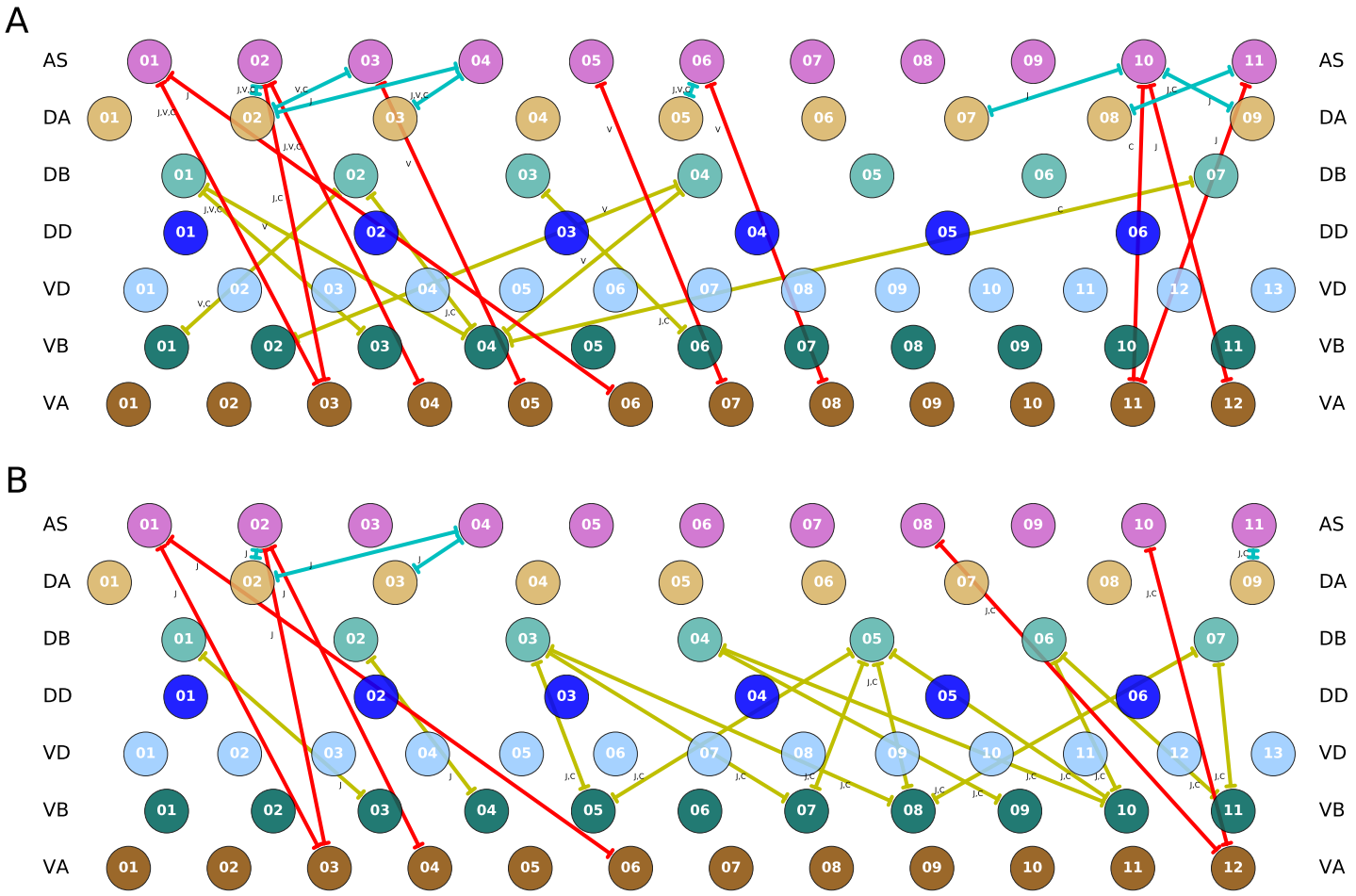

Figure 9. Key interunit gap junctions present in the *C. elegans* connectome for the hermaphrodite [A] and the male [B]. Gap junctions are color coded based on the pair of motoneurons they connect, as in previous figures: VBI–IDB in yellow, DAI–IAS in green, and ASI–IVA in red. Connections shown are present in one or several of the main datasets. For the hermaphrodite, each connection is marked as appearing in one or more of the following three datasets: j (***Jarrell et al., 2012***), v (***Varshney et al., 2011***), or c (***Cook et al., 2019***). For the male, each connection is marked as appearing in one or more of the following two datasets: j (***Jarrell et al., 2012***), or c (***Cook et al., 2019***).

2018; ***Xu et al., 2018***). Analysis of representative solutions revealed a number of key insights. First, the models demonstrate that oscillations can be generated in a small subcircuit within each subunit of the model. This CPG mechanism is consistent with previous modeling work (***Olivares et al., 2018***). Ultimately, only an update in the ventral nerve cord anatomical reconstruction (***Mulcahy et al., 2018***; ***Cook et al., 2019***) will make the quest for the feasibility of network oscillators more reliable. Second, the models demonstrate that coordination across neural units in the VNC can be achieved by a single electrical synapse, and that any of the interunit gap junctions are sufficient to generate the necessary coordination. Third, the models demonstrate that coordination can be achieved in either the anterior or posterior direction, and some solutions coordinate in both directions. Through an analysis of the ensemble of the 15 filtered solutions, we identify not one but several novel mechanisms for coordinating oscillations across neighboring neural units, without relying on stretch-receptor feedback or neural pacemakers.

In ***Xu et al.*** (***2018***), three mechanisms were proposed to work synergistically to drive and propagate a coordinated undulatory wave from the head to the tail: (1) proprioceptive coupling between B-type motor neurons; (2) AVB-B gap junction coupling; and (3) weak electrical coupling between motoneurons. Xu et al., examined primarily the second mechanism for coordinating the wave propagation. However, their results do not eliminate the possibility of the gap junctions as a coordination mechanism. The main result of this model is the demonstration that this mechanism is indeed sufficient to coordinate anteroposterior coordination. Furthermore, we demonstrate that these gap junctions can coordinate the different oscillators in either/both directions: anteriorly and posteriorly. The solutions that we selected to analyze in detail were deliberately chosen because of their simplicity. Part of this simplicity allowed us to identify a gap junction for posterior coordination and a gap junction for anterior coordination. Solutions that use both gap junctions have the potential to coordinate activity in both directions: from head to tail and vice-versa.

Until recently, the role of motorneuron AS in locomotion had gone largely unexamined. Our previous work suggested the theoretical plausibility of the involvement of AS in the generation of oscillations and in the dorso-ventral coordination of oscillations (***Olivares et al., 2018***). This was followed closely by experiments providing evidence that AS indeed plays a role in forward locomotion (***Tolstenkov et al., 2018***). Specifically, they observed that animals with ablated AS motoneurons retained their ability to move, but crawled with lower speed, and an overall distorted undulation. That ablation of AS motoneurons does not abolish body undulations entirely, indicates that there are mechanisms that can generate oscillations independently of AS. If the possibility that the worm has multiple mechanisms for generating and coordinating undulations is open, then showing that ablating one component does not affect the generation does not lead to the conclusion that therefore that component must not be involved in generating oscillations. In this work, AS is again involved in the generation and dorso-ventral coordination of oscillations. Theoretical results raise an important unexplored possibility: Could the worm still generate and coordinate undulatory oscillations in the absence of stretch receptors and intrinsic oscillations in neurons? If so, the AS motorneuron is a likely candidate to play a role. This avenue has not been explored experimentally yet.

It has been proposed that generating intrinsic network oscillations is difficult because the network would have to rely extensively on inhibitory connections (***Cohen and Denham, 2019***). However, in this work and in our previous work (***Olivares et al., 2018***), the evolutionary search revealed multiple instantiations of possibilities over a wide range of the inhibition/excitation spectrum. In this study, for example, seven out of the 15 solutions contained a majority of excitatory synapses. Furthermore, across the 15 models analyzed, it is possible to find one with any of its six chemical synapses in an excitatory configuration. This suggests a wide range of possibilities for the feasibility of network oscillations in the ventral nerve cord. Ultimately, to the degree that specific connections in the VNC are demonstrated to be excitatory and inhibitory, the feasibility of such network oscillators must be reexamined.

Analysis of the solutions revealed how different internal mechanisms of oscillation generation

can produce similar behaviors. Specifically, analysis of the solutions demonstrated that a wide range of different phase shifts between neurons within the subunit could lead to similar phase shifts across different subunits and ultimately to very similar forward locomotion behavior. This is an interesting proof of concept that the same network structure, with different network parameters, can nevertheless converge on functionally relevant aspects of the behavior.

Despite the breadth of knowledge available about the connectome, the worm's nervous system remains highly underconstrained. Our approach takes this issue seriously, generating multiple possible hypotheses for how different patterns of activity could lead to the observed behavior. The strength and uniqueness of the approach is that it integrates connectomic and behavioral data to infer candidate configurations of synaptic properties. As experiments that map neural manipulations to behavioral kinematics increases and the data becomes public and standardized, these can be used to further constrain the optimization search and thereby hone in on the space of candidate models (***Izquierdo, 2018***).

Model and Methods

The Model

We model a repeating unit of the ventral nerve cord based on a statistical analysis of the available connectome data (***Haspel and O'Donovan, 2011***). The neurons drive a muscle model based on the anatomical reconstructions of the worm, replicated in previous modeling work (***Izquierdo and Beer, 2018***). The muscles, in turn, drive a biomechanical model of the body situated in an agar environment, based on previous modeling work (***Boyle et al., 2012***). In order to examine the feasibility of multiple CPGs to produce forward locomotion, the current model does not include stretch-receptor feedback and it does not allow for the possibility of motoneurons to be pacemaker neurons. In this section, we describe each of the components of the model. The complete model, the evolutionary algorithm, and the tools of analysis are available online: https://github.com/edizquierdo/MultipleNetworkOscillator.

Environment

In the laboratory, *C. elegans* is typically grown and studied in petri dishes containing a layer of agar gel. The gel is firm and worms tend to lie on the surface. The experiments in this paper focus on worm locomotion on this surface. Given the low Reynolds number physics of *C. elegans* locomotion, inertial forces can be neglected and the resistive forces of the medium can be well-approximated as a linear drag $F = -Cv$ (***Boyle et al., 2012***; ***Boyle, 2009***; ***Cohen and Boyle, 2010***; ***Niebur and Erdös, 1991***).The tangential and normal drag coefficients for agar used in this model were taken from those reported in (***Berri et al., 2009***) and used in the model of the body that this work builds on (***Boyle et al., 2012***): $C_{\parallel} = 3.2 \times 10^{-3}$ kg$\cdot s^{-1}$ and $C_{\perp} = 128 \times 10^{-3}$ kg$\cdot s^{-1}$, respectively (***Boyle et al., 2012***; ***Boyle, 2009***; ***Lighthill, 1976***; ***Niebur and Erdös, 1991***; ***Wallace, 1969***; ***Berri et al., 2009***).

Body

The model of the body is a reimplementation of the model presented by ***Boyle et al.*** (***2012***). Because when placed on an agar surface, the worm locomotes by bending only in the dorsal-ventral plane, the worm body is modeled in 2D cross-section. The ~1mm long continuous body of the worm is divided into variable-width discrete segments. Each segment is bounded by two cross-sectional rigid rods. The endpoints of the rods are connected to their neighbors via damped spring lateral elements modeling the stretch resistance of the cuticle. The endpoints of the rods are also connected to the adjacent rods on the opposite side via damped spring diagonal elements modeling the compression resistance of internal pressure. The rest lengths, spring constants and damping constants of the lateral and diagonal elements are taken directly from previous work (***Boyle et al., 2012***), which in turn estimated them from experiments with anesthetized worms (***Sauvage, 2007***). The forces from the lateral and diagonal elements are summed at the endpoints of the rods and then the equations of motion are written for the center of mass of each rod. Since each rod has two translational (x,

y) and one rotational (ϕ) degrees of freedom, the body model has a total of $3(N_{\text{seg}}+1)$ degrees of freedom. The current model has $N_{\text{seg}} = 50$, so a total of 153 degrees of freedom. The full set of expressions for forces, as well as all kinematic and dynamic parameters are identical to those in previous work (***Boyle, 2009***; ***Boyle et al., 2012***).

Muscles

Body wall muscles in the worm are arranged as staggered pairs in four bundles around the body (***Waterston, 1988***; ***Altun and Hall, 2009***). These muscles can contract and relax in the dorsoventral plane. Following previous work (***Izquierdo and Beer, 2018***), muscles are modeled as elements that lie along the cuticle (Fig. 1). The force of each muscle is distributed across all lateral elements that they intersect. Because adjacent body wall muscles overlap one another in *C. elegans*, multiple muscles can exert force on the same lateral elements. Since the model is 2D, we combine right and left bundles into a single set of 24 dorsal and 24 ventral muscles. Muscle forces are modeled as a function of muscle activation and mechanical state using simplified Hill-like force-length and force-velocity properties (***Hill, 1938***).

Following previous work (***Boyle et al., 2012***; ***Izquierdo and Beer, 2018***), muscle activation is modeled as a leaky integrator with a characteristic time scale ($\tau_{\text{M}} = 100$ms), which agrees with response times of obliquely striated muscle (***Milligan et al., 1997***). The muscle activation is represented by the unitless variable A_m^k that evolves according to:

$$\frac{dA_m^k}{dt} = \frac{1}{\tau_M}(I_m^k - A_m^k) \tag{1}$$

where A_m^k is the total current driving dorsal and ventral ($k = \{D, V\}$) muscles along the body ($m = 1, .., 24$). Also following previous modeling work (***Boyle et al., 2012***) and experimental evidence that electrical coupling between body wall muscle cells plays only a restricted role for *C. elegans* body bend propagation (***Leifer et al., 2011***; ***Wen et al., 2012***), inter-muscle electrical coupling is assumed to be too weak and therefore not included in the model.

Ventral nerve cord circuit

As connectome data is incomplete for the ventral nerve cord (***White et al., 1986***; ***Varshney et al., 2011***; ***Cook et al., 2019***), we relied on a statistical analysis of the motoneurons in relation to the position of the muscles they innervate to model the repeating neural unit along the VNC (***Haspel and O'Donovan, 2011***). We modeled the VNC as a neural network composed of seven identical subunits (Fig. 1). The anatomy of the repeating subunit was grounded on previous theoretical work, where we demonstrated that a subset of the components present in the statistically repeating unit found in the dataset were sufficient to generate dorsoventral oscillations (***Olivares et al., 2018***). The minimal configuration found in that work included motorneurons: AS, DA, DB, VD, VA, and VB; and chemical synapses: DA→DB, DB→AS, AS→DA, AS→VD, VD→VA, and VD→VB. Given that the subunits need to coordinate their oscillations with neighboring subunits in order to produce forward locomotion, we added the following connections to adjacent neural subunits found in the statistical analysis of the VNC (***Haspel and O'Donovan, 2011***): AS⊣VA^{+1}, DA⊣AS^{+1}, VB⊣DB^{+1}, where the superscript $+1$ indicates that the neuron is part of the posterior subunit. We use this notation to refer to interunit connections only; for intraunit connections we leave the superscript out. The minimal configuration found in previous work (***Olivares et al., 2018***) did not include motoneuron DD because of the lack of outgoing connections to the rest of the motoneurons within the unit, and therefore its unlikeliness to be involved in the generation of network oscillations. As the current model involves a neuromuscular system, and DD has neuromuscular junctions that allow it to drive the muscles of the worm, we included it. We also included the connections to and from DD present in the statistical analysis of the VNC (***Haspel and O'Donovan, 2011***), including intraunit connections: DA→DD, VA→DD, VB→DD, and VD⊣DD; and interunit connections: DB→DD^{+1}, and VA^{+1} →DD.

Dorsal and ventral motoneurons in each unit drive the dorsal and ventral body wall muscles adjacent to them, respectively. The input to the body wall muscles is represented by variable I_m^k,

such that:

$$I_m^k = \sum_{i \in N^k} \gamma_m q_i S_i \tag{2}$$

where k denotes whether the body wall muscle is dorsal or ventral ($k = \{D, V\}$) and m denotes the position of the muscle along the body ($m = 1, .., 24$), the set N^k corresponds to the dorsal/ventral motoneurons, {AS, DA, DB, DD}, {VA, VB, VD} respectively. Following previous work (***Boyle et al., 2012***), an anterior-posterior gradient in the maximum muscle efficacies is implemented by a linearly (posteriorly) decreasing factor, $\gamma_m = 0.7\,(1 - (((m-1)F)/M))$, where γ_m is the efficacy for neuroumuscular junctions connecting motoneurons to muscle m, and F is the anteroposterior gain in muscle contraction. q_i corresponds to the neuromuscular junction strength from motorneuron i. Because AS-, A-, and B-class motoneurons are known to be cholinergic and therefore excitatory and the D-class motoneurons are GABAergic and therefore inhibitory (***McIntire et al., 1993***; ***Rand et al., 1997***), we constrained the signs of their neuromuscular junctions accordingly. Finally, S_i corresponds to the synaptic output for each motorneuron.

Neural model

Following electrophysiological studies in *C. elegans* (***Goodman et al., 1998***; ***Mellem et al., 2008***) and previous modeling efforts (***Izquierdo and Lockery, 2010***; ***Izquierdo and Beer, 2013***, ***2018***), motoneurons were modeled as nodes with simple first order nonlinear dynamics (***Beer, 1995***),

$$\tau_i \frac{dV_i}{dt} = -V_i + \sum_{j=1}^{N} w_{ji}\sigma(V_j + \theta_j) + \sum_{j=1}^{N} g_{ji}(V_j - V_i) \tag{3}$$

where V_i represents the membrane potential of the ith neuron relative to its resting potential. The time-constant of the neuron is represented by τ_i. The model assumes chemical synapses release neurotransmitter tonically and that steady-state synaptic activity is a sigmoidal function of presynaptic voltage (***Kuramochi and Doi, 2017***; ***Lindsay et al., 2011***; ***Wicks et al., 1996***), $\sigma(x) = 1/(1 + e^{-x})$. θ_j is a bias term that shifts the range of sensitivity of the output function. The synaptic weight from neuron j to neuron i is represented by w_{ji}. In line with previous theoretical work (***Wicks et al., 1996***; ***Izquierdo and Beer, 2013***; ***Kunert et al., 2017***), the electrical synapses were modeled as bidirectional ohmic resistances, with g_{ji} as the conductance between cell i and j ($g_{ji} > 0$). The indices i and j used for the chemical synapses and the gap junctions represent each of the motoneurons in the circuit (AS, DA, DB, VD, VA, and VB) and the specific connectivity between them is given by the neuroanatomy (Fig. 1). Self-connections were included in the chemical synapses term to allow for the functional equivalent of active membrane conductances which have been reported for *C. elegans* neck muscle motor neurons (***Goodman et al., 1998***). This allows the neural model to reproduce the variety of graded activity that has been described in the free-living nematode *Caenorhabditis elegans* (***Goodman et al., 1998***; ***Lindsay et al., 2011***; ***Mellem et al., 2008***; ***Liu et al., 2009***). Specifically, by changing the strength of the self-connection on each neuron, that model neuron can be either smoothly depolarized or hyperpolarized from a tonic resting potential (***Mellem et al., 2008***), or bistable, with nonlinear transitions between a resting potential and a depolarized potential (***Goodman et al., 1998***).

Numerical methods

The model was implemented in C++. The neural model was solved by Forward Euler method of integration with a 0.5ms step. The body model was solved using a Semi-Implicit Backward Euler method with a 0.1ms step.

Optimization strategy

As the parameters for physiological properties of neurons and synapses involved in forward locomotion in *C. elegans* are largely unknown, we used an evolutionary algorithm to search through

the space of parameters for configurations that could produce forward movement without stretch-receptors.

Evolutionary algorithm

Unknown model parameters were adjusted using a real-valued evolutionary algorithm. A naive parameterization of our model would contain around 300 neural parameters. However, it makes little sense to work directly with such a large set of unconstrained parameters. Instead, we imposed a variety of symmetries on the model in order to reduce the number of parameters. We assumed that the parameters in each repeating VNC neural unit were identical and that neurons belonging to the same class had identical parameters. Altogether, the model was reduced to a total of 42 free parameters. There are 26 parameters that describe each of the 7 neuron classes and neuromuscular junctions: 7 biases, 7 time-constants, 7 self-connections, and 5 neuromuscular junctions. There are 15 parameters that describe the strength and polarity of the connections: 10 weights for intraunit connections: 9 chemical synapses (AS→DA, AS→VD, DA→DB, DB→AS, VD→VA, VD→VB, DA→DD, VB→DD, VA→DD) and one electrical synapse (VD⊣DD); 5 weights for interunit connections: 2 chemical synapses (VA→DD^{-1}, DB→DD^{+1}) and 3 gap junctions (DA⊣AS^{+1}, VI⊣DB^{+1}, AS⊣VA^{+1}). One additional parameter, F, describes the anteroposterior gain in muscle contraction.

Fitness function

Preliminary results established that evolving the complete neuromechanical model to generate locomotion from scratch did not produce results reliably. In order to increase the rate of success in the search process, we used an incremental approach to the optimization procedure. The incremental approach involved two stages. During the first stage, we evolved a single VNC neural unit, isolated from the body and environment, to oscillate (Fig. 10A). Specifically, the fitness function required that the B-class motoneurons oscillate and that the oscillation frequency matched what has been observed for body bending in crawling worms:

$$F_1 = \prod_{j \in \{\mathrm{DB},\mathrm{VB}\}} \left(\frac{2}{A * T} \int_0^T \left| \frac{dS_j}{dt} \right| dt \right) \left(1 - \frac{|f_j - f_\mathrm{a}|}{f_\mathrm{a}} \right) \tag{4}$$

where A corresponds to a oscillation amplitude threshold ($A = 0.5$), S_j corresponds to the output of the motoneuron, T corresponds to the duration of the simulation, f_j is the frequency of neuron j, and f_a is the frequency of bending in the worm ($f_\mathrm{a} = 0.44$Hz (***Cohen et al., 2012***)). The first component of this fitness function is aimed at encouraging oscillatory activity by maximizing the rate of change of neural activity in DB and VB. The contribution from this component was capped to a value of 1. The second component of this fitness function is aimed at matching the frequency of the worm.

The second stage of the optimization procedure started when the evolving population reached a fitness threshold above 0.99 (out of a maximum of 1) on the first stage. During the second stage, the isolated neural unit was integrated back into the complete neuromechanical model and evolved to move forward (Fig. 10B). Specifically, the evolving neural unit was integrated with the rest of the units in the VNC. The parameters of the rest of the units were made identical to those of the evolving unit. Interunit connections and neuromuscular junctions to the muscles were incorporated into the model, so as to drive the body and generate forces against the environment. The fitness function was extended from the first stage to include a component that encouraged model worms to match the forward velocity of the worm on agar:

$$F_2 = F_1 \left(1 - \frac{|\overline{V} - V_\mathrm{a}|}{V_\mathrm{a}} \right) \tag{5}$$

where $\overline{V}$ corresponds to the average velocity of the model worm over the duration of the simulation, and V_a corresponds to the average forward velocity of the worm on agar ($V_\mathrm{a} = 0.22$ mm/s) (***Cronin et al., 2005***).

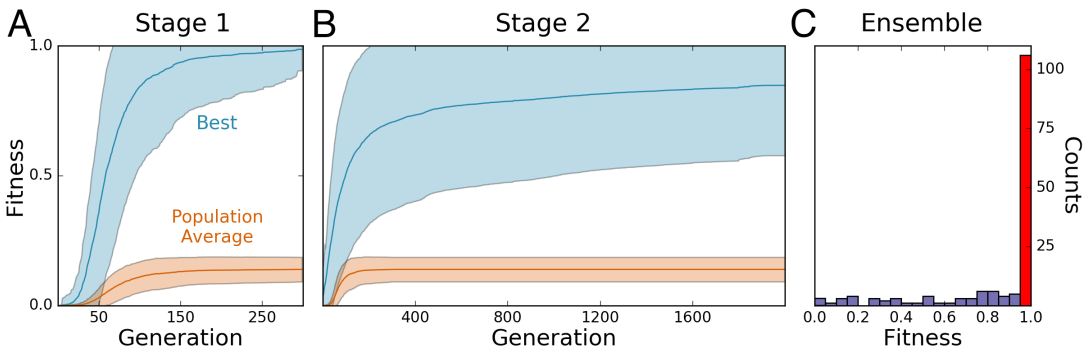

Figure 10. Optimization strategy reliably finds model configurations that match worm forward locomotion. [A] Optimization of an isolated neural unit so as to match B-class neuron oscillation and frequency. [B] Optimization of the full neuromechanical model so as to match B-class neuron oscillation and frequency and model worm instantaneous velocity. The fitness of the best individual in the population over generations, averaged across all evolutionary runs, is shown in blue. The standard deviation is shown in a lighter shade of blue. The average fitness of the individuals in the population over generations, averaged across all evolutionary runs, is shown in orange. Standard deviation shown in a lighter shade of orange. [C] Distribution of best final fitness across evolutionary runs. 65% of the evolutionary searches found a solution with a fitness greater than 0.95 (red bar).

Evolutionary searches

Evolutionary searches reliably found model configurations that matched worm forward locomotion. We ran 160 independent searches with different random seeds. Of these, 104 solutions (65%) reached a fitness greater than 0.95 on the final stage (Fig. 10C). Upon examination, all 104 successful solutions exhibited locomotory behavior that resembled forward crawling in the worm.

Filtering strategy

All 104 evolved solutions moved with the body bending frequency and mean velocity that was targeted during the evolutionary search. In order to focus on the subset of solutions that resemble as closely as possible forward locomotion in *C. elegans*, we filtered this set of solutions to those that matched a set of locomotion features that were not imposed during the evolutionary search. We applied the following three criteria: (a) Relative role of the different neuron classes in forward locomotion, (b) body curvature and (c) trajectory curvature. Altogether, 15 solutions fulfilled all three filtering criteria (Fig. 11D). We discuss each of the criteria in turn.

Relative role of the different neuron classes in forward locomotion

A- and B-class neurons have been implicated in backward and forward locomotion, respectively, through ablations performed at the larval stage, when only DA and DB neurons are present (***Chalfie et al., 1985***). Specifically, these studies reveal that ablating B-class motorneurons prevents forward locomotion but not backward, and that ablating A-class motorneurons prevents backward but not forward locomotion (***Chalfie et al., 1985***). More recently, optical imaging studies in the adult have shown that both A- and B-class motoneurons are active during locomotion, but that the activity of B-class motorneurons is higher during forward locomotion than the activity of A-class motorneurons, and vice-versa during backward locomotion (***Faumont et al., 2011***; ***Kawano et al., 2011***; ***Haspel et al., 2010***). In all evolved solutions of our model, both A and B-class motoneurons are active during forward locomotion. In order to focus only on the solutions where the B-class input to muscles is necessary to produce forward locomotion but not the A-class, we simulated each solution while eliminating the neuromuscular junctions from B-class motoneurons and from A-class motoneurons, independently. We then evaluated the velocities of the model worms as a result of this manipulation (Fig. 11A). We selected solutions that met the following two criteria: (1) eliminating the A-class neuromuscular junction does not seriously compromise locomotion (i.e.,

velocity greater than 20% of target velocity); and (2) eliminating the B-class neuromuscular junction does compromise forward locomotion (i.e., velocity less than 20% of target velocity). A total of 74 solutions fulfilled both criteria.

Body curvature

In addition to the frequency of the body bends, there are a number of other features of the kinematics of movement during forward locomotion that have been characterized (***Berri et al., 2009***; ***Fang-Yen et al., 2010***; ***Cronin et al., 2005***; ***Lebois et al., 2012***; ***Pierce-Shimomura et al., 2008***; ***Yemini et al., 2013***; ***Vidal-Gadea et al., 2011***; ***Karbowski et al., 2008***; ***Butler et al., 2015***; ***Cohen et al., 2012***; ***Wen et al., 2012***; ***Xu et al., 2018***). We further filtered our solutions based on two features: the body-bending wavelength, and the anteroposterior curvature profile. Measurements of the wavelength of the body bends in the worm fall in the range of 0.4 to 0.9 body length (***Berri et al., 2009***; ***Fang-Yen et al., 2010***; ***Cronin et al., 2005***; ***Lebois et al., 2012***; ***Pierce-Shimomura et al., 2008***; ***Yemini et al., 2013***; ***Vidal-Gadea et al., 2011***; ***Karbowski et al., 2008***; ***Butler et al., 2015***; ***Cohen et al., 2012***). We evaluated the body wavelength in all solutions and selected those that fell within the observe range (Fig. 11B). The anteroposterior curvature profile corresponds to the relative amount of curvature along the body axis and has been shown to be more pronounced near the head of the worm than the tail (***Wen et al., 2012***; ***Xu et al., 2018***). We evaluated the mean curvature in the anteroposterior axis in all solutions and selected those with a negative slope in the linear regression that fit the curvature profile (Fig. 11B). Altogether, we narrowed down the 104 solutions to 30 that fulfilled both criteria (Fig. 11D).

Trajectory curvature

The translational direction of *C. elegans* during forward locomotion tends to be relatively straight, with only a small degree of curvature in the absence of stimuli (***McIntire et al., 1993***; ***Peliti et al., 2013***). In the evolved model worms, the straightness in the trajectory was not optimized, so the distribution of curvature in the translational trajectory is broad (Fig. 11C). In order to filter out model worms that curved much more than the worm during forward locomotion, we set a threshold of 1 mm in trajectory curvature radius (Fig. 11C) and we found 77 solutions that moved as straight as the worm (Fig. 11D), even in the absence of proprioceptive or sensory feedback.

Acknowledgments

The work in this paper was supported by National Science Foundation Grant IIS-1524647.

References

Abbott LF. Theoretical Neuroscience Rising. Neuron. 2008; 60(3):489 – 495. doi: https://doi.org/10.1016/j.neuron.2008.10.019.

Altun Z, Hall D. Muscle system, somatic muscle. WormAtlas Edited for the web by Laura A Herndon Last revision: May. 2009; 31:2013. https://www.wormatlas.org/.

Arshavsky Y, Deliagina T, Orlovsky G. Central pattern generators: mechanisms of operation and their role in controlling automatic movements. Neuroscience and Behavioral Physiology. 2016; 46(6):696–718. doi: https://doi.org/10.1007/s11055-016-0299-5.

Beer RD. On the dynamics of small continuous-time recurrent neural networks. Adaptive Behavior. 1995; 3(4):469–509. doi: https://doi.org/10.1177/105971239500300405.

Berri S, Boyle JH, Tassieri M, Hope IA, Cohen N. Forward locomotion of the nematode *C. elegans* is achieved through modulation of a single gait. HFSP Journal. 2009; 3(3):186–193. doi: https://doi.org/10.2976/1.3082260.

Boyle JH. *C. elegans* locomotion: an integrated approach. PhD thesis, University of Leeds; 2009.

Boyle JH, Berri S, Cohen N. Gait modulation in *C. elegans*: an integrated neuromechanical model. Frontiers in Computational Neuroscience. 2012; 6:10. doi: https://doi.org/10.3389/fncom.2012.00010.

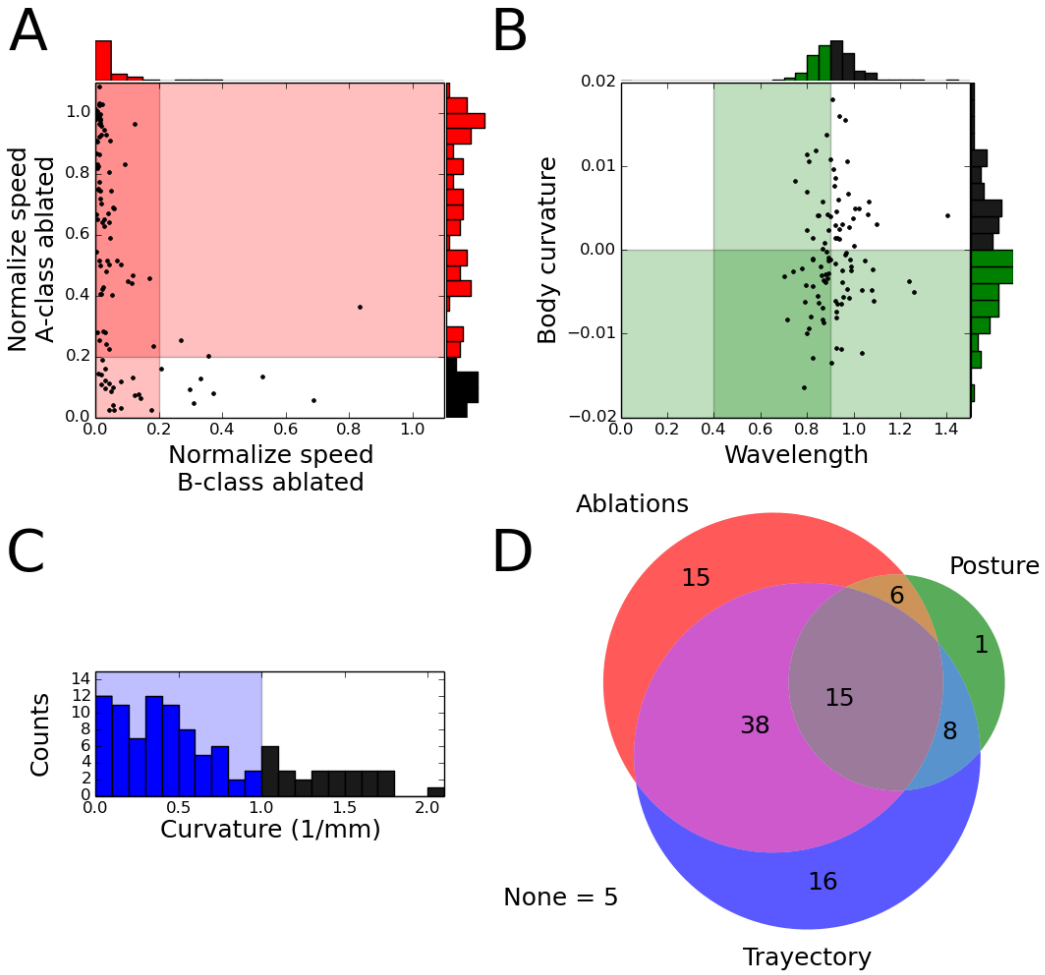

Figure 11. Filtering solutions to include only those that most closely match what is known about locomotion in the worm. [A] Relative role of the different neuron classes in forward locomotion. Proportion of the forward locomotion speed maintained by each model worm when the neuromuscular junction from the B-class motoneurons (x-axis) or the A-class motoneurons (y-axis) are ablated. Each point in the figure represents a single solution. Solutions in the shaded region represent those that match the filtering criteria: (1) Ablation to A-class neuromuscular junctions should not impair forward locomotion entirely; and (2) Ablation to B-class neuromuscular junctions should impair forward locomotion performance. [B] Body curvature. Measures of the model worms' anteriorposterior curvature profile (x-axis) and their body wavelength (y-axis). Green shaded areas represent biologically plausible ranges. In the previous two figures, solutions in the darkest shaded region represent those that match both criteria. Histograms are shown for the criteria on each axis. [C] Trajectory curvature. Distribution of curvature radius for the center of mass over time. The blue shaded area represents solutions with a relatively straight trajectory. [D] Venn diagram representing the distribution of the 104 selected solutions according to the fulfillment of the three different filters: relative role of different neural classes in red, body curvature in green, and trajectory curvature in blue. We focus our analysis on the 15 solutions that matched all criteria.

Butler VJ, Branicky R, Yemini E, Liewald JF, Gottschalk A, Kerr RA, Chklovskii DB, Schafer WR. A consistent muscle activation strategy underlies crawling and swimming in *Caenorhabditis elegans*. Journal of the Royal Society Interface. 2015; 12(102):20140963. doi: https://doi.org/10.1098/rsif.2014.0963.

Chalfie M, Sulston JE, White JG, Southgate E, Thomson JN, Brenner S. The neural circuit for touch sensitivity in *Caenorhabditis elegans*. The Journal of neuroscience. 1985; 5(4):956–964. doi: https://doi.org/10.1523/JNEUROSCI.05-04-00956.1985.

Chiel HJ, Beer RD. The brain has a body: adaptive behavior emerges from interactions of nervous system, body and environment. Trends in Neurosciences. 1997; 20(12):553 – 557. doi: https://doi.org/10.1016/S0166-2236(97)01149-1.

Chiel HJ, Ting LH, Ekeberg Ö, Hartmann MJZ. The brain in its body: motor control and sensing in a biomechanical context. Journal of Neuroscience. 2009; 29(41):12807–12814. doi: https://doi.org/10.1523/JNEUROSCI.3338-09.2009.

Cohen E, Yemini E, Schafer W, Feitelson DG, Treinin M. Locomotion analysis identifies roles of mechanosensory neurons in governing locomotion dynamics of *C. elegans*. Journal of Experimental Biology. 2012; 215(20):3639–3648. doi: https://doi.org/10.1242/jeb.075416.

Cohen N, Boyle JH. Swimming at low Reynolds number: a beginners guide to undulatory locomotion. Contemporary Physics. 2010; 51(2):103–123. doi: https://doi.org/10.1080/00107510903268381.

Cohen N, Denham JE. Whole animal modeling: piecing together nematode locomotion. Current Opinion in Systems Biology. 2019; 13:150 – 160. doi: https://doi.org/10.1016/j.coisb.2018.12.002.

Cohen N, Sanders T. Nematode locomotion: dissecting the neuronal–environmental loop. Current opinion in neurobiology. 2014; 25:99–106. doi: https://doi.org/10.1016/j.conb.2013.12.003.

Cook SJ, Jarrell TA, Brittin CA, Wang Y, Bloniarz AE, Yakovlev MA, Nguyen KCQ, Tang LTH, Bayer EA, Duerr JS, Bülow HE, Hobert O, Hall DH, Emmons SW. Whole-animal connectomes of both *Caenorhabditis elegans* sexes. Nature. 2019; 571(7763):63–71. doi: https://doi.org/10.1038/s41586-019-1352-7.

Cronin CJ, Mendel JE, Mukhtar S, Kim YM, Stirbl RC, Bruck J, Sternberg PW. An automated system for measuring parameters of nematode sinusoidal movement. BMC genetics. 2005; 6(1):5. doi: https://doi.org/10.1186/1471-2156-6-5.

Dasen JS. Evolution of locomotor rhythms. Trends in neurosciences. 2018; 41(10):648–651. doi: https://doi.org/10.1016/j.tins.2018.07.013.

Deng X, Xu JX. A 3D undulatory locomotion model inspired by *C. elegans* through DNN approach. Neurocomputing. 2014; 131:248–264. doi: https://doi.org/10.1016/j.neucom.2013.10.019.

Denham JE, Ranner T, Cohen N. Signatures of proprioceptive control in *Caenorhabditis elegans* locomotion. Philosophical Transactions of the Royal Society B: Biological Sciences. 2018; 373(1758):20180208. doi: https://doi.org/10.1098/rstb.2018.0208.

Fang-Yen C, Wyart M, Xie J, Kawai R, Kodger T, Chen S, Wen Q, Samuel AD. Biomechanical analysis of gait adaptation in the nematode *Caenorhabditis elegans*. Proceedings of the National Academy of Sciences. 2010; 107(47):20323–20328. doi: https://doi.org/10.1073/pnas.1003016107.

Faumont S, Rondeau G, Thiele TR, Lawton KJ, McCormick KE, Sottile M, Griesbeck O, Heckscher ES, Roberts WM, Doe CQ, et al. An image-free opto-mechanical system for creating virtual environments and imaging neuronal activity in freely moving *Caenorhabditis elegans*. PLoS One. 2011; 6(9):e24666. doi: https://doi.org/10.1371/journal.pone.0024666.

Fieseler C, Kunert-Graf J, Kutz JN. The control structure of the nematode *Caenorhabditis elegans*: Neuro-sensory integration and proprioceptive feedback. Journal of Biomechanics. 2018; 74:1–8. doi: https://doi.org/10.1016/j.jbiomech.2018.03.046.

Fouad AD, Teng S, Mark JR, Liu A, Alvarez-Illera P, Ji H, Du A, Bhirgoo PD, Cornblath E, Guan SA, et al. Distributed rhythm generators underlie *Caenorhabditis elegans* forward locomotion. Elife. 2018; 7:e29913. doi: https://doi.org/10.7554/eLife.29913.

Gao S, Guan SA, Fouad AD, Meng J, Kawano T, Huang YC, Li Y, Alcaire S, Hung W, Lu Y, et al. Excitatory motor neurons are local oscillators for backward locomotion. Elife. 2018; 7:e29915. doi: https://doi.org/10.7554/eLife.29915.

Gjorgjieva J, Biron D, Haspel G. Neurobiology of *Caenorhabditis elegans* locomotion: where do We Stand? Bioscience. 2014; 64(6):476–486. doi: https://doi.org/10.1093/biosci/biu058.

Gleeson P, Lung D, Grosu R, Hasani R, Larson SD. c302: a multiscale framework for modelling the nervous system of *Caenorhabditis elegans*. Philosophical Transactions of the Royal Society B: Biological Sciences. 2018; 373(1758):20170379. doi: https://doi.org/10.1098/rstb.2017.0379.

Goodman MB, Hall DH, Avery L, Lockery SR. Active Currents Regulate Sensitivity and Dynamic Range in *C. elegans* Neurons. Neuron. 1998; 20(4):763 – 772. doi: https://doi.org/10.1016/S0896-6273(00)81014-4.

Goulding M. Circuits controlling vertebrate locomotion: moving in a new direction. Nature Reviews Neuroscience. 2009; 10(507). doi: https://doi.org/10.1038/nrn2608.

Haspel G, O'Donovan MJ. A perimotor framework reveals functional segmentation in the motoneuronal network controlling locomotion in *Caenorhabditis elegans*. The Journal of Neuroscience. 2011; 31(41):14611–14623. doi: https://doi.org/10.1523/JNEUROSCI.2186-11.2011.

Haspel G, O'Donovan MJ, Hart AC. Motoneurons dedicated to either forward or backward locomotion in the nematode *Caenorhabditis elegans*. The Journal of Neuroscience. 2010; 30(33):11151–11156. doi: https://doi.org/10.1523/JNEUROSCI.2244-10.2010.

Hill AV. The heat of shortening and the dynamic constants of muscle. Proc R Soc Lond B. 1938; 126(843):136–195. doi: https://doi.org/10.1098/rspb.1938.0050.

Ijspeert AJ. Central pattern generators for locomotion control in animals and robots: a review. Neural Networks. 2008; 21(4):642–653. doi: 10.1016/j.neunet.2008.03.014.

Izquierdo EJ. Role of simulation models in understanding the generation of behavior in *C. elegans*. Current Opinion in Systems Biology. 2018; doi: https://doi.org/10.1016/j.coisb.2018.11.003.

Izquierdo EJ, Beer RD. From head to tail: a neuromechanical model of forward locomotion in *Caenorhabditis elegans*. Philosophical Transactions of the Royal Society B: Biological Sciences. 2018; 373(1758):20170374. doi: https://doi.org/10.1098/rstb.2017.0374.

Izquierdo E, Beer R. Connecting a connectome to behavior: an ensemble of neuroanatomical models of *C. elegans* klinotaxis. PLoS Computational Biology. 2013; 9(2):e1002890. doi: https://doi.org/10.1371/journal.pcbi.1002890.

Izquierdo E, Lockery S. Evolution and analysis of minimal neural circuits for klinotaxis in *Caenorhabditis elegans*. Journal of Neuroscience. 2010; 30(39):12908–12917. doi: https://doi.org/10.1523/JNEUROSCI.2606-10.2010.

Jarrell TA, Wang Y, Bloniarz AE, Brittin CA, Xu M, Thomson JN, Albertson DG, Hall DH, Emmons SW. The connectome of a decision-making neural network. Science. 2012; 337(6093):437–444. doi: https://doi.org/10.1126/science.1221762.

Karbowski J, Schindelman G, Cronin CJ, Seah A, Sternberg PW. Systems level circuit model of *C. elegans* undulatory locomotion: mathematical modeling and molecular genetics. Journal of Computational Neuroscience. 2008; 24(3):253–276. doi: https://doi.org/10.1007/s10827-007-0054-6.

Katz PS. Evolution of central pattern generators and rhythmic behaviours. Philosophical Transactions of the Royal Society B: Biological Sciences. 2016; 371(1685):20150057. doi: https://doi.org/10.1098/rstb.2015.0057.

Kawano T, Po MD, Gao S, Leung G, Ryu WS, Zhen M. An imbalancing act: gap junctions reduce the backward motor circuit activity to bias *C. elegans* for forward locomotion. Neuron. 2011; 72(4):572–586. doi: https://doi.org/10.1016/j.neuron.2011.09.005.

Krakauer JW, Ghazanfar AA, Gomez-Marin A, MacIver MA, Poeppel D. Neuroscience Needs Behavior: Correcting a Reductionist Bias. Neuron. 2017; 93(3):480 – 490. doi: https://doi.org/10.1016/j.neuron.2016.12.041.

Kunert J, Shlizerman E, Kutz JN. Low-dimensional functionality of complex network dynamics: Neurosensory integration in the *Caenorhabditis elegans* connectome. Physical Review E. 2014; 89(5):052805. doi: https://doi.org/10.1103/PhysRevE.89.052805.

Kunert J, Proctor J, Brunton S, Kutz J. Spatiotemporal Feedback and Network Structure Drive and Encode *Caenorhabditis elegans* Locomotion. PLoS Computational Biology. 2017; 13(1):e1005303. doi: https://doi.org/10.1371/journal.pcbi.1005303.

Kuramochi M, Doi M. A computational model based on multi-regional calcium imaging represents the spatio-temporal dynamics in a *Caenorhabditis elegans* sensory neuron. PLoS One. 2017; 12(1):e0168415. doi: https://doi.org/10.1371/journal.pone.0168415.

Lebois F, Sauvage P, Py C, Cardoso O, Ladoux B, Hersen P, Di Meglio JM. Locomotion control of *Caenorhabditis elegans* through confinement. Biophysical Journal. 2012; 102(12):2791–2798. doi: https://doi.org/10.1016/j.bpj.2012.04.051.

Leifer AM, Fang-Yen C, Gershow M, Alkema MJ, Samuel AD. Optogenetic manipulation of neural activity in freely moving *Caenorhabditis elegans*. Nature Methods. 2011; 8(2):147. doi: https://doi.org/10.1038/nmeth.1554.

Lighthill J. Flagellar hydrodynamics. SIAM review. 1976; 18(2):161–230. doi: https://doi.org/10.1137/1018040.

Lindsay TH, Thiele TR, Lockery SR. Optogenetic analysis of synaptic transmission in the central nervous system of the nematode *Caenorhabditis elegans*. Nat Commun. 2011; 2(306). doi: https://doi.org/10.1038/ncomms1304.

Liu Q, Hollopeter G, Jorgensen EM. Graded synaptic transmission at the *Caenorhabditis elegans* neuromuscular junction. Proceedings of the National Academy of Sciences. 2009; 106(26):10823–10828. doi: https://doi.org/10.1073/pnas.0903570106.

Machino K, Link CD, Wang S, Murakami H, Murakami S. A semi-automated motion-tracking analysis of locomotion speed in the *C. elegans* transgenics overexpressing beta-amyloid in neurons. Frontiers in Genetics. 2014; 5:202. doi: https://doi.org/10.3389/fgene.2014.00202.

Mailler R, Avery J, Graves J, Willy N. A biologically accurate 3d model of the locomotion of *Caenorhabditis elegans*. In: *Biosciences (BIOSCIENCESWORLD), 2010 International Conference on* IEEE; 2010. p. 84–90. doi: https://doi.org/10.1109/BioSciencesWorld.2010.18.

Marder E, Bucher D. Central pattern generators and the control of rhythmic movements. Current Biology. 2001; 11(23):R986 – R996. doi: https://doi.org/10.1016/S0960-9822(01)00581-4.

McIntire SL, Jorgensen E, Kaplan J, Horvitz HR. The GABAergic nervous system of *Caenorhabditis elegans*. Nature. 1993; 364(6435):337. doi: https://doi.org/10.1038/364337a0.

Mellem JE, Brockie PJ, Madsen DM, Maricq AV. Action potentials contribute to neuronal signaling in *C. elegans*. Nature Neuroscience. 2008; 11(8):865–867. doi: https://doi.org/10.1038/nn.2131.

Milligan B, Curtin N, Bone Q. Contractile properties of obliquely striated muscle from the mantle of squid (Alloteuthis subulata) and cuttlefish (Sepia officinalis). Journal of Experimental Biology. 1997; 200(18):2425–2436. https://jeb.biologists.org/content/200/18/2425.

Minassian K, Hofstoetter US, Dzeladini F, Guertin PA, Ijspeert A. The human central pattern generator for locomotion: Does it exist and contribute to walking? The Neuroscientist. 2017; 23(6):649–663. doi: https://doi.org/10.1177/1073858417699790.

Mulcahy B, Witvliet D, Holmyard D, Mitchell J, Chisholm AD, Samuel AD, Zhen M. A Pipeline for Volume Electron Microscopy of the *Caenorhabditis elegans* Nervous System. Frontiers in Neural Circuits. 2018; 12. doi: https://doi.org/10.3389/fncir.2018.00094.

Niebur E, Erdös P. Theory of the locomotion of nematodes: Dynamics of undulatory progression on a surface. Biophysical Journal. 1991; 60(5):1132–1146. doi: https://doi.org/10.1016/S0006-3495(91)82149-X.

Olivares EO, Izquierdo EJ, Beer RD. Potential role of a ventral nerve cord central pattern generator in forward and backward locomotion in *Caenorhabditis elegans*. Network Neuroscience. 2018; 2(3):323–343. doi: https://doi.org/10.1162/netn_a_00036.

Omura DT, Clark DA, Samuel AD, Horvitz HR. Dopamine signaling is essential for precise rates of locomotion by *C. elegans*. PLoS One. 2012; 7(6):e38649. doi: https://doi.org/10.1371/journal.pone.0038649.

Palyanov A, Khayrulin S, Larson SD. Three-dimensional simulation of the *Caenorhabditis elegans* body and muscle cells in liquid and gel environments for behavioural analysis. Philosophical Transactions of the Royal Society B: Biological Sciences. 2018; 373(1758):20170376. doi: https://doi.org/10.1098/rstb.2017.0376.

Peliti M, Chuang JS, Shaham S. Directional locomotion of *C. elegans* in the absence of external stimuli. PLoS One. 2013; 8(11):e78535. doi: https://doi.org/10.1371/journal.pone.0078535.

Pierce-Shimomura JT, Chen BL, Mun JJ, Ho R, Sarkis R, McIntire SL. Genetic analysis of crawling and swimming locomotory patterns in *C. elegans*. Proceedings of the National Academy of Sciences. 2008; 105(52):20982–20987. doi: https://doi.org/10.1073/pnas.0810359105.

Rand JB, Duerr JS, Frisby DL. Neurogenetics of Synaptic Transmission in *Caenorhabditis elegans*. In: *Advances in Pharmacology*, vol. 42 Elsevier; 1997.p. 940–944. doi: https://doi.org/10.1016/S1054-3589(08)60902-3.

Rossignol S, Dubuc R, Gossard JP. Dynamic sensorimotor interactions in locomotion. Physiological Reviews. 2006; 86(1):89–154. doi: https://doi.org/10.1152/physrev.00028.2005, pMID: 16371596.

Sauvage P. Etude de la locomotion chez *C. elegans* et perturbations mecaniques du mouvement. PhD thesis, PhD dissertation, Laboratoire Matiere et Systemes Compiexes (Paris, France: Universite Paris Diderot-Paris 7); 2007.

Shen XN, Sznitman J, Krajacic P, Lamitina T, Arratia P. Undulatory locomotion of *Caenorhabditis elegans* on wet surfaces. Biophysical Journal. 2012; 102(12):2772–2781. doi: https://doi.org/10.1016/j.bpj.2012.05.012.

Tavernarakis N, Shreffler W, Wang S, Driscoll M. unc-8, a DEG/ENaC family member, encodes a subunit of a candidate mechanically gated channel that modulates *C. elegans* locomotion. Neuron. 1997; 18(1):107 – 119. doi: https://doi.org/10.1016/S0896-6273(01)80050-7.

Tolstenkov O, Van der Auwera P, Costa WS, Bazhanova O, Gemeinhardt TM, Bergs AC, Gottschalk A. Functionally asymmetric motor neurons contribute to coordinating locomotion of *Caenorhabditis elegans*. eLife. 2018; 7:e34997. doi: https://doi.org/10.7554/eLife.34997.

Varshney L, Chen B, Paniagua E, Hall D, Chklovskii D. Structural properties of the *Caenorhabditis elegans* neuronal network. PLoS Computational Biology. 2011; 7(2):e1001066. doi: https://doi.org/10.1371/journal.pcbi.1001066.

Vidal-Gadea A, Topper S, Young L, Crisp A, Kressin L, Elbel E, Maples T, Brauner M, Erbguth K, Axelrod A, et al. *Caenorhabditis elegans* selects distinct crawling and swimming gaits via dopamine and serotonin. Proceedings of the National Academy of Sciences. 2011; 108(42):17504–17509. doi: https://doi.org/10.1073/pnas.1108673108.

Wallace H. Wave formation by infective larvae of the plant parasitic nematode Meloidogyne javanica. Nematologica. 1969; 15(1):65–75. doi: https://doi.org/10.1163/187529269X00100.

Waterston R. Muscle. In: Wood W, editor. *The nematode C. elegans* New York: Cold Spring Harbor Laboratory Press; 1988.p. 281–335.

Wen Q, Gao S, Zhen M. *Caenorhabditis elegans* excitatory ventral cord motor neurons derive rhythm for body undulation. Philosophical Transactions of the Royal Society B: Biological Sciences. 2018; 373(1758):20170370. doi: https://doi.org/10.1098/rstb.2017.0370.

Wen Q, Po MD, Hulme E, Chen S, Liu X, Kwok SW, Gershow M, Leifer AM, Butler V, Fang-Yen C, et al. Proprioceptive coupling within motor neurons drives *C. elegans* forward locomotion. Neuron. 2012; 76(4):750–761. doi: https://doi.org/10.1016/j.neuron.2012.08.039.

White J, Southgate E, Thomson J, Brenner S. The structure of the nervous system of the nematode *Caenorhabditis elegans*. Philosophical Transactions of the Royal Society B: Biological Sciences. 1986; 275(938):327–348. doi: https://doi.org/10.1098/rstb.1986.0056.

Wicks SR, Roehrig CJ, Rankin CH. A dynamic network simulation of the nematode tap withdrawal circuit: predictions concerning synaptic function using behavioral criteria. J Neurosci. 1996; 16(12):4017–4031. doi: https://doi.org/10.1523/JNEUROSCI.16-12-04017.1996.

Xu M, Jarrell TA, Wang Y, Cook SJ, Hall DH, Emmons SW. Computer assisted assembly of connectomes from electron micrographs: application to *Caenorhabditis elegans*. PLoS One. 2013; 8(1):e54050. doi: https://doi.org/10.1371/journal.pone.0054050.

Xu T, Huo J, Shao S, Po M, Kawano T, Lu Y, Wu M, Zhen M, Wen Q. Descending pathway facilitates undulatory wave propagation in *Caenorhabditis elegans* through gap junctions. Proceedings of the National Academy of Sciences. 2018; 115(19):E4493–E4502. doi: https://doi.org/10.1073/pnas.1717022115.

Yemini E, Jucikas T, Grundy LJ, Brown AE, Schafer WR. A database of *Caenorhabditis elegans* behavioral phenotypes. Nature Methods. 2013; 10(9):877. doi: https://doi.org/10.1038/nmeth.2560.

Zhen M, Samuel AD. *C. elegans* locomotion: small circuits, complex functions. Current Opinion Neurobiology. 2015; 33:117–126. doi: https://doi.org/10.1016/j.conb.2015.03.009.